Aceh Int. J. Sci. Technol., 10(2) 128-138
August, 2021
doi: 10.13170/aijst.10.2.21982

Aceh International Journal of Science and Technology
ISSN: p-2088-9860; e-2503-2398
Journal homepage: http://jurnal.unsyiah.ac.id/aijst

Effect of Silica Addition on Mechanical Properties of Eggshell-Derived Hydroxyapatite

Fatma[1], Desnelli[1], Fahma Riyanti[1,2], Mustafa Kamal[3], Muhammad Ramdan Abdul Mannan[4], Poedji Loekitowati Hariani[1,2,*]

[1] Department of Chemistry, Faculty of Mathematics and Natural Sciences, Universitas Sriwijaya, Indralaya, Indonesia;
[2] Research Centre of Advanced Material and Nanocomposite, Faculty of Mathematics and Natural Sciences, Universitas Sriwijaya, Indralaya, Indonesia ;
[3] Department of Biology, Faculty of Mathematics and Natural Sciences, Universitas Sriwijaya, Indralaya, Indonesia;
[4]Bachelor Program of Chemistry, Faculty of Mathematics and Natural Sciences, Universitas Sriwijaya, Indralaya, Indonesia
*Corresponding author email: puji_lukitowati@mipa.unsri.ac.id

Received : August 1, 2021
Accepted : September 17, 2021
Online : September 18, 2021

Abstract –Eggshell is a solid waste that is available in abundance but is being left unused. Eggshell containing calcium in a high amount. Calcium can be used as a precursor for hydroxyapatite (HAp). Modification of HAp with SiO_2 is expected to improve its low mechanical properties for biomedical applications. In this study, HAp is synthesized from the eggshell. Then, it was modified by adding SiO_2 utilizing the coprecipitation method with concentrations of 10%, 20%, 30%, and 40%, respectively. The HAp and HAp/SiO_2 were characterized using; X-ray diffraction and Fourier transform infrared spectroscopy. The analysis HAp and HAp/SiO_2 were density, compressive strength, and hardness. The best mechanical properties of HAp/SiO_2 were characterized using SEM-EDS. The HAp were prepared successfully with a ratio of Ca/P was 1.673, close to the theoretical 1.67. The addition of SiO_2 caused a decrease in crystallite size and density but increased compressive strength and hardness. The best mechanical properties of HAp/SiO_2 were obtained with SiO_2 of 30% and 40% with similar values.

Keywords: Eggshell, hydroxyapatite, SiO_2, mechanical properties

Introduction

Hydroxyapatite (HAp) is one of the materials that has received considerable attention for its potential to apply in various applications, including biomedical products (Gomes *et al.*, 2019), drug delivery (Taha *et al.*, 2020), and skin regeneration (Pal *et al.*, 2020). Besides, it is also promising in waste treatment (Ibrahim *et al.*, 2020; Hariani *et al.*, 2020) and heterogeneous catalysts (Saha *et al.*, 2018). HAp has the molecular formula $Ca_{10}(PO_4)6(OH)_2$, which belongs to the type of apatite material compound $[M_{10}(XO_4)6Z_2]$, which has a crystal phase of the most stable polycrystalline calcium phosphate compound (Wang *et al.*, 2017). The molar ratio of calcium to phosphorus (Ca/P) is about 1.67.

HAp is also beneficial for bone tissue engineering applications such as bio-scaffolds (Xiao *et al.*, 2019), bioactive glasses (Bazli *et al.*, 2017), bioceramics (Hubadillah *et al.*, 2020), and implants (Shakir *et al.*, 2018). It is similar to human bones and teeth in crystal structure and composition (Xu *et al.*, 2004; Amaechi *et al.*, 2019). HAp is applicable in biomedicine because it has high biocompatibility (Aktug *et al.*, 2017), osteoconductivity (Bovand *et al.*, 2019), and bioactivity (Szczes *et al.*, 2017), and is non-inflammatory, non-immunogenic, and non-

toxic (Dan *et al.*, 2019; Coelho *et al.*, 2019). Its ability to absorb hydrophilic and hydrophobic compounds is vital in drug delivery and environmental applications (Barbosa *et al.*, 2020). However, HAp has shortcomings, especially in the medical field. It has low mechanical properties, namely the low strength due to the influence of the applied compressive and tensile forces (Noviyanti *et al.*, 2021), its relatively slow reactivity, and integration with cells (Bohner, 2009; Latifi, 2012). Synthetic HAp has mechanical properties poorer than human cortical bone's (Hsu *et al.*, 2021). The application of HAp in the medical field must meet certain standard parameters, including good mechanical properties (Chakrawaty *et al.*, 2020). Structural modifications such as substituting or incorporating other materials can increase mechanical strength (Noviyanti *et al.*, 2021) and improve the quality of tissue repair. Several researchers have modified HAp with other materials such as magnesium (Noviyanti *et al.*, 2021), chitosan (Pighinelli and Kucharska, 2013), chloride (Hsu *et al.*, 2021), and zirconia (Es-saddik *et al.*, 2021).

Several researchers have modified HAp by adding silica. The addition of silica can improve Hap's mechanical properties and increase in vivo bioactivity (Latifi, 2012). Silica is biocompatible and non-toxic (Sadeghazade *et al.*, 2015; Thian *et al.*, 2006). Latifi (2012) reported synthesizing HAp/SiO_2 with silica with 20% and 40% concentrations and finding that increasing SiO_2 concentration can decrease crystallinity. Hydroxyapatite is synthesized from the reaction of phosphoric pentoxide with calcium nitrate tetrahydrate in an alcohol medium. The other research that synthesized HAp/SiO_2 by mechanical alloying followed by sintering showed that increasing SiO_2 concentration increased densification, mechanical properties, and in vitro bioactivity of HAp/SiO_2 nanocomposite sintered at 900 °C (Taha *et al.*, 2020).

Hydroxyapatite can be synthesized from raw materials or solid wastes that are readily available in quantity, such as fish bones (Pamungkas *et al.*, 2019), clamshells (Pu'ad *et al.*, 2019), eggshells (Noviyanti *et al.*, 2021), camel bones (Alqodami *et al.*, 2018), and animal bones (Obada *et al.*, 2020). One of the potential sources for HAp is chicken eggshells. Chicken eggs are usually used in large quantities in the food industry, restaurants, households, and even the pharmaceutical industry (Curkovi*et al.*, 2017). An eggshell, which accounts for about 11% of the egg's weight, is almost always disposed of as solid waste. The main element is calcium carbonate (95–97 wt%) with a minor amount of calcium phosphate, magnesium carbonate, organic, strontium, sodium, iron, potassium, and chlorine (Witoon, 2011; Curkovic *et al.*, 2017). The high calcium content in chicken eggshells is the potential to be used as HAp material.

In this study, HAp was synthesized with CaO that originated from chicken eggshells. The reaction of CaO with H_3PO_4 produces HAp. Later, HAp was modified with SiO_2 at various concentrations with the coprecipitation method. This method is a simple, inexpensive, and high success (Curkovic *et al.*, 2017). The resulting HAp and HAp/SiO_2 were characterized using XRD, FTIR, and SEM-EDS. The effect of SiO_2 concentration was determined by the density and mechanical tests, including compressive strength and hardness.

Materials and Methods

Materials

The materials used were chicken eggshells (Hyline brown chicken) from local chicken farmers in Palembang city, chemicals including H_3PO_4, TEOS ($C_8H_{20}O_4Si$), NH_4OH obtained from Sigma Aldrich (Germany), and distilled water.

HAp Preparation

Eggshells were cleaned using distilled water until free of impurities. The clean eggshells were boiled for ±1 hour, separated from the membrane, and dried in the sun for a day. After being dried, they were mashed with a grinding machine to be a fine powder of ±100 mesh. A total of 100 g of the eggshell powder obtained was calcined at around 900 °C for 3 hours at a speed of 10°/min to change the $CaCO_3$ phase into CaO. The calcined CaO was added with 250 mL of deionized water, stirred using a magnetic stirrer for 30 minutes. Then, 250 mL of 1 M H_3PO_4 was added slowly while being stirred. The reaction produced HAp. The HAp produced was dried at a temperature of 105°C using an oven for 1 hour (Hariani *et al.*, 2020; Asadipour *et al.*, 2019).

HAp/SiO_2 Preparation

The preparation of HAp/SiO_2 in this study refers to the procedure reported by Asadipour et al. (2019). In preparing HAp/SiO_2, TEOS was used as a precursor with different weights to obtain SiO_2 with 10%, 20%,

30%, and 40% concentrations. Each mixture of HAp and TEOS solutions was added with 1 M ammonia solution gradually until the pH of the solution lies between 9-11 while stirred with a magnetic stirrer and given a stream of nitrogen gas. The mixture was allowed to stand for about 96 hours, then filtered and washed with deionized water. The powder obtained was dried using an oven at 40 °C for 72 hours. The reaction of calcium hydroxide with phosphoric acid produced HAp, as follows (Curkovic *et al.*, 2017):

$$CaCO_3 \rightarrow CaO + CO_2 \quad (1)$$

$$CaO + H_2O \rightarrow Ca(OH)_2 \quad (2)$$

$$10Ca(OH)_2 + 6H_3PO_4 \rightarrow Ca_{10}(PO_4)(OH)_2 + 18H_2O \quad (3)$$

The reaction of SiO_2 formation from the precursor TEOS was as follows:

$$Si(OC_2H_5)_4 + 2H_2O \rightarrow SiO_2 + 4C_2H_5OH \quad (4)$$

Characterization of HAp and HAp/SiO_2

The HAp and HAp/SiO_2 were characterized using X-ray diffraction (XRD Malvern Panalytical) using Cu-Kα = 0.154 nm, in the range 2θ of 5-80°. The HAp and HAp/SiO_2 functional groups were identified using the Fourier transform infrared (FTIR Prestige 21) instrument at a wavenumber of 400-4000 cm^{-1}. A scanning electron microscope-energy dispersive spectrometer (SEM-EDS JOEL JSM 6510 LA) was used to observe the morphology and composition of the elements.

Analysis of Density, Compressive Strenght, and Hardness

Density (ρ) was analyzed using the ratio of mass divided by total volume m/v (g/cm^3), while the compressive strength was tested used the Autograph SHIMADZU AG-10 TE, Vickers Hardness Test (Leco M-400-H1).

Results

Characterization of HAp/SiO_2 using XRD and FTIR

Figure 1 shows the XRD spectra of HAp and HAp/SiO_2, with varying concentrations of SiO_2. The XRD analysis was performed at 2θ = 5-80°. The crystallite size HAp and HAp/SiO_2 were determined using Scheerer's equation, according to the following formula:

$$D = \frac{K\lambda}{\beta \cos\theta} \quad (5)$$

Where D is the crystallite size (nm), K s the Scherrer constant (0.91), λ is the wavelength of X-rays (1.54056Å), β is the value of Full Width at Half Maximum (rad), and θ is the diffraction angle (FWHM) (rad). Table 1 shows Crystallite sizes of HAp and HAp/SiO_2. From the table, it can be seen that the greater the concentration of SiO_2, the smaller the crystallite size. Figure 1 shows the diffractograms of HAp and HAp/SiO_2.

Table 1. Crystallite sizes of HAp and HAp/SiO_2

SiO_2 content (%)	The average crystallite size (nm)
0	51.8
10	47.8
20	39.4
30	35.7
40	34.8

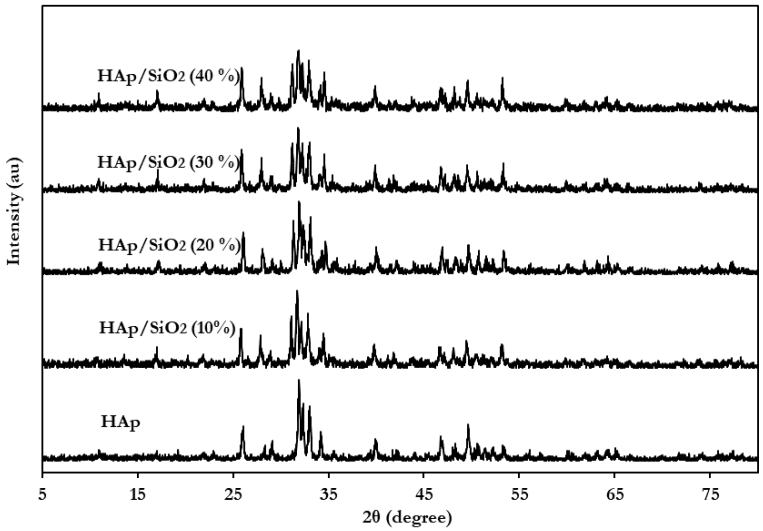

Figure 1. XRD patterns of HAp and HAp/SiO_2

Figure 2 shows the FTIR spectra of HAp and HAp/SiO_2 at wavenumbers 400-4000 cm^{-1}. All peaks indicate the similarity of phosphate functional groups observed at wavenumbers 900-1200 cm^{-1} (Hariani *et al.*, 2020). There are OH groups on a wide peak at wavenumbers 3280-3600 cm^{-1} (Balamurugan *et al.*, 2013). Symmetric stretching vibrating bands of Si-O-Si were observed at a wavenumber of about 800 cm^{-1}. The addition of SiO_2 causes changes in peak intensity, especially those identified at wavenumbers below 800 cm^{-1}.

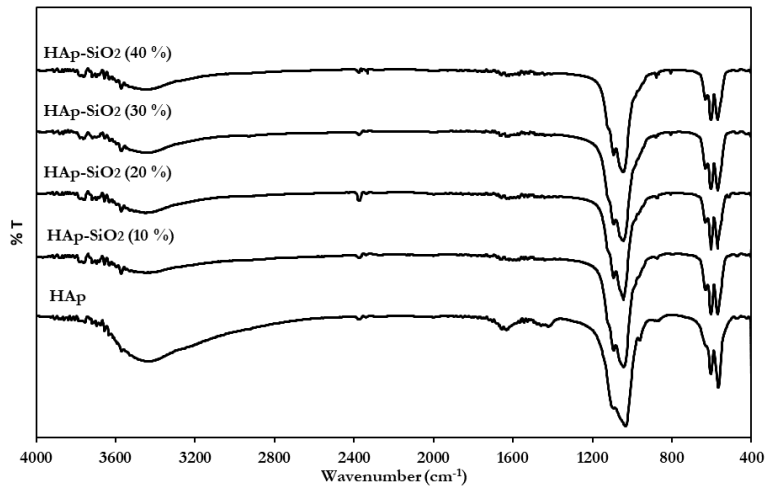

Figure 2. FTIR spectra of HAp dan HAp/SiO_2

Density, Compressive Strength, Hardness of HAp and HAp/SiO_2

Figure 3 shows the density of HAp and HAp/SiO_2 that decreased along with the addition of SiO_2. Compressive strength and hardness are critical properties of a material to be compatible with biomedical biomaterials. Figures 4 and 5 indicate the compressive strength and hardness values of HAp and HAp/SiO_2.

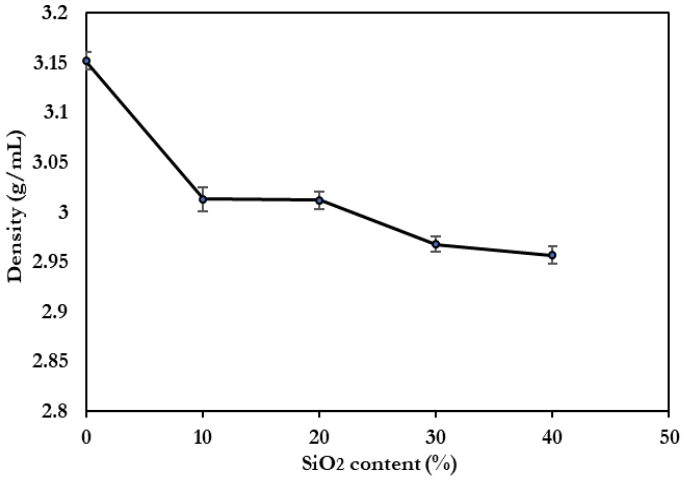

Figure 3. The density of HAp and HAp/SiO_2 at different SiO_2 content

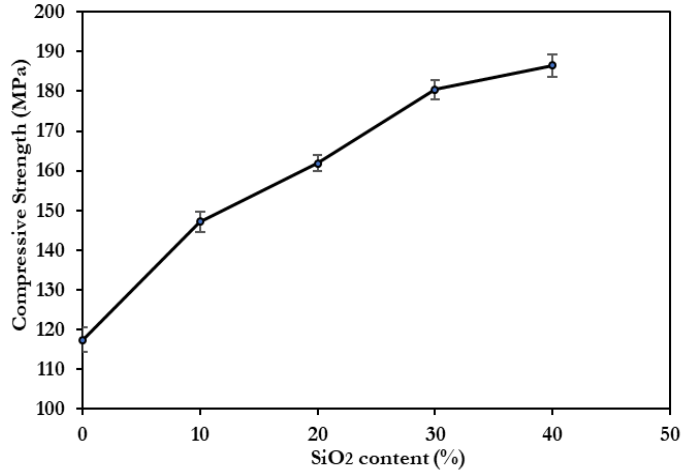

Figure 4. Compressive strength of HAp and HAp/SiO_2 at different SiO_2 content

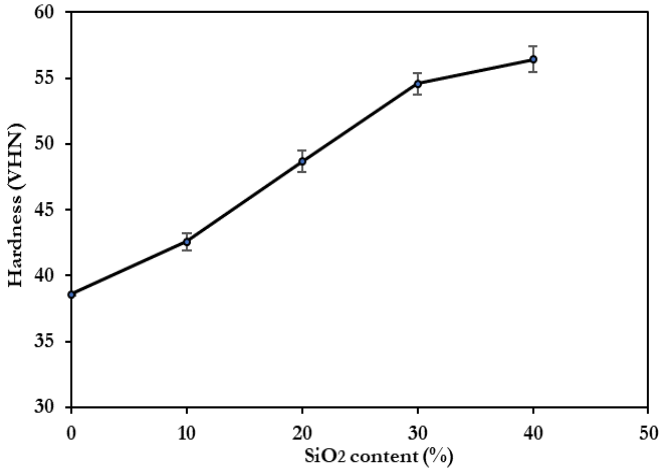

Figure 5. The hardness of HAp and HAp/SiO_2 at different SiO_2 content

SEM-EDS Characterization of HAp and HAp/SiO_2

In this study, SEM-EDS analysis was performed on HAp and HAp/SiO_2 (30%). HAp/SiO_2 (30%) was selected because both HAp/SiO_2 (30%) and HAp/SiO_2 (40%) show the best result with similar mechanical properties. Figure 6 shows the morphologies of HAp and HAp/SiO_2 with the addition of 30% SiO_2 as measured by a magnification of 5000 x. The compositions of HAp and HAp/SiO_2 based on EDS results are presented in Table 2.

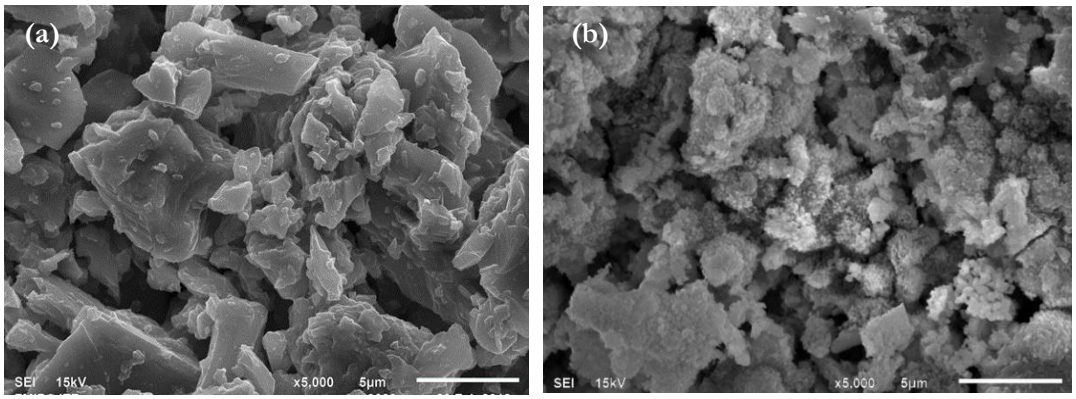

Figure 6. Morphologies of (a) HAp and (b) HAp/SiO_2 (30%)

Table 2. Compositions of elements of HAp dan HAp/SiO_2 (30%)

Elements	Percentage (%)	
	HAp	HAp-SiO_2 (30 %)
O	45.16	46.08
P	17.36	12.70
Ca	37.48	27.45
Si	-	13.77

Discussion

Characterization of HAp and HAp/SiO_2 using XRD and FTIR

According to JCPDS No. 09-432, HAp has a major peak at 2θ 25.879°, 31.773°, 32.196°, 32.902°, and 49.468°. The HAp manufactured from chicken eggshells appears to agree with these data, namely at 2θ angles at 25.52° (201), 31.94° (211), 32.22° (112), 32.98° (300), and 49.66° (213). The addition of SiO_2 caused the peaks to widen and the intensity to decrease, as seen at the 2θ around 31-32° (Figure 1). The amorphous nature of silica causes silica peaks not to be observed. Silica peaks should be observed at 2θ around 23° (Hariani et al., 2020). The increasing silica content in HAp brought the crystallite size to decrease, indicating the amorphous silica phase in the composite (Latifi, 2012), which caused a decrease in intensity. Table 1 shows the average crystallite sizes of HAp and HAp/SiO_2 calculated based on Scheerer's equation. Based on the table, the higher the SiO_2 content, the smaller the crystallite size. The research by Hanora *et al.* (2021) showed that the greater the concentration of SiO_2 (25%, 30%, 40%, and 50%), the smaller the crystal size. In this study, the crystallite sizes of HAp and HAp/SiO_2 are small (< 100 nm).

The characterization of HAp and HAp/SiO_2 using FTIR shows the peaks of HAp and HAp added with SiO_2 of 10%, 20%, 30%, and 40% contained OH groups, as identified at wavenumbers 3421.7 cm^{-1}, 3435.2 cm^{-1}, 3431.6 cm^{-1}, 3435.2 cm^{-1}, and 3431.4 cm^{-1}. These hydroxyapatite structures containing OH groups. Besides that, OH groups could also be from water molecules absorbed. The peak also strengthened the presence of H_2O in HAp at 1622.4 cm^{-1}. The presence of phosphate groups (PO_4^{3-}) in HAp could be identified at wavenumbers 1032.8 cm^{-1}, 960.5 cm^{-1}, and 565.1 cm^{-1}. The peak also appeared in HAp/SiO_2, but the intensity

decreased. Peaks that indicate the presence of Si-O-Si asymmetric stretching groups in HAp/SiO_2 can be identified in wavenumbers 1070.5 cm^{-1}, 1072.4 cm^{-1}, 1072.6 cm^{-1}, and 1070.5 cm^{-1}.

Density, compressive strength, and hardness of HAp and HAp/SiO_2

The statistical tests using ANOVA and LSD showed that the density of HAp was significantly different from that of HAp/SiO_2, while HAp/SiO_2 with the addition of 10-40% of SiO_2 was not significantly different. Theoretically, the density of HAp is 3.156 g/cm^3 (Ramesh *et al.*, 2013). Taha *et al.* (2020) reported that the density of SiO_2 was 2.65 g/cm^3, and that of HAp prepared by the mechanochemical synthesis method was 3.15 g/cm^3. Jouda *et al.* (2021) obtained a density of HAp from the cow bone of 2.982 g/cm^3 and was considered compatible with biomedical applications. The density values of HAp and HAp/SiO_2 are similar to previous researchers, namely between 2.957-3.152 g/cm^3.

The mechanical properties determined included compressive strength and hardness, as shown in Figures 4 and 5. In Figures 4 and 5, it can be seen that the addition of SiO_2 to HAp increased both compressive strength and hardness. The statistical tests using ANOVA and LSD test showed that the compressive strength of HAp/SiO_2 with variations in SiO_2 concentration also showed significant differences. The nature of silica can improve the brittleness of hydroxyapatite (Kailasanathan and Gangadharan, 2016). The compressive strength values for human compact bone are in the range of 170-193 MPa. HAp/SiO_2 with concentrations of 30% and 40% met these criteria. The compressive strength values were included in the compressive strength value of cortical bone, ranging from 100 to 230 MPa (Ficai *et al.*, 2011). In this study, the compressive strength of HAp/SiO_2 with concentrations of 30% and 40% were 180.44 ± 2.55 MPa and 186.5 ± 3.12 MPa, respectively.

The hardness of materials that will experience frictional force and plastic deformation should be known. Plastic deformation is the condition of a material in which the microstructure of the material cannot return to its original shape when given a force. The HAp and HAp/SiO_2 hardness tests showed that the addition of SiO_2 increased the hardness (Figure 5). The SiO_2 added filled the HAp pores. If the porosity is too high, the biomaterial will be easily porous because many pore cavities are formed.

In contrast, low porosity will inhibit the intake of nutrients from the blood vessels to the bones. According to Jouda (2021), the value of hardness is highly dependent on density and porosity. Hardness values of cortical bones range from 53.7 to 77.9 VHN (Ahn *et al.*, 2001; Rho *et al.*, 1997). In this study, the hardness values of HAp/SiO_2 with SiO_2 compositions of 30% and 40% met these criteria. The statistical tests using ANOVA and LSD test showed that HAp with the addition of SiO_2 of 30% and 40% were not significantly different obtained 54.56 ± 0.83 VHN and 56.43 ± 0.98 VHN, respectively. The best properties of the compressive strength and hardness values of HAp/SiO_2 were achieved at 30% and 40%.

Characterization of HAp and HAp/SiO_2 using SEM-EDS

HAp and HAp/SiO_2 with the addition of 30% SiO_2 were analyzed using SEM-EDS, as shown in Figure 6. The results of EDS are presented in Table 2. The surface morphologies of HAp and HAp/SiO_2 are different from each other. HAp has an oval shape; its surface becomes tighter with the addition of SiO_2 because SiO_2 fills the pores of HAp. The molar ratio of calcium to phosphorus in HAp was 1.673, close to the theoretical ratio of 1.67, indicating the synthesis of HAp has been successful. The addition of SiO_2 by 30% increase the Si element and decreased the P and Ca elements with a molar ratio of Ca/P = 1.670. The elements of HAp/SiO_2 was O=43.08, P = 12.70, Ca= 27.45 and Si= 13.77%.

Conclusion

The synthesis of hydroxyapatite (HAp) from eggshells and its modification by SiO_2 with concentrations of 10%, 20%, 30%, and 40% have been carried out. The HAp obtained had a Ca/P ratio of 1.673. The addition of SiO_2 reduced the average crystallite size and density. The modification also improved the mechanical properties of HAp by increasing its compressive strength and hardness. The concentration of SiO_2 for the best mechanical properties were achieved at 30% and 40% with a similar value. It can be reckoned that eggshell-derived HAp with SiO_2 modification has the potential as a biomaterial for biomedical applications.

Acknowledgment

The research was funded by DIPA of Universitas Sriwijaya (Hibah Kompetitif Universitas Sriwijaya of 2021 with Contract No.0010/UN9/SK.LP2M.PT/2021).

References

Ahn, E.S., Gleason, N.J. Nakahira, A. and Ying, I.Y. 2001. Nanostructure processing of hydroxyapatite-based bioceramics. Nano Letters, 1(3): 1325-1330.

Aktug, S.L., Durdu, S. Yalcin, E. Cavusoglu, K. and Usta, M. 2017. Bioactivity and biocompatibilityof hydroxyapatite-based bioceramic coatings on zirconium by plasma electrolytic oxidation. Materials Science and Engineering: C, 71: 1020-1027.

Alqadami, A.A., Khan, M.A. Otero, M. Siddiqui, M.R. Jeon, B.H. and Batoo, K.M. 2018. A magnetic product nanocomposite produced from camel bones for efficient adsorption of toxic metals from water. Journal of Cleaner Production, 178: 293-304.

Amaechi, B.T., AbdulAzees, P.A. Alshareif, D.O. Shehata, M.A. Lima, P.P.de.C.S, Abdollahi, A. Kalkhorani, P.S. and Evans, V. 2019. Comparative hydroxyapatite efficacy of a hydroxyapatite and a fluoride toothpaste for prevention and remineralization of dental caries in children. BDJ Open, 5(1): 1-9.

Asadipour, K., Nezafati, N. Nourbakhsh, M.S. Ardakani, M.H. and Bohlooli, S. 2019. Characterization and biological properties of a novel synthesized silicon-substituted hydroxyapatite deriver from eggshell. The Internasional Journal of Artificial Organs, 42(2): 95-108.

Balamurugan, A., Kannan, S. and Rajeswari, S. 2002. Synthesis of hydroxyapatite on silica surface by using glyserin as a drying control chemical additive. Materials Letters, 57: 1244-1250.

Barbosa, A.A., Junior, S.A. Mendes, R.L. de Lima, R.S. and Ferraz, A.de.V. 2020. Multifunctional hydroxyapatite with potential for application in theranostic nanomedicine. Materials Science and Engineering: C, 116: 1-8.

Bazli, L., Eftekhari, Y. and Khavandi, A. 2017. Preparation and characterization of Sn-containing glasses for brachytherapy application. Trans Indian Ceram Soc. 76(4): 242-246.

Tan, F., Zhu, Y. Ma, Z. and Al-Rubeai, M. 2020. Recent advances in implant-based drug delivery in otorhinolaryngology. Acta Biomaterialia. 198: 46-55.

Bohner, M. 2009. Silicon-substituted calcium phosphates- a critical view. Biomaterials 30(32): 6403-6406

Bovand, D., Allazadeh, M.R. Rasouli, S. Khodadad, E. and Borhani, E. 2019. Studying the effect of hydroxyapatite particles in osteoconductivity of Ti-HA bioceramic. Journal of the Australian Ceramic Society, 55(2): 395-403.

Chakrawaty, J., Rabbi, M.F. Chalivendra, V. Ferreira, T. and Brigham, C.J. 2020. Mechanical and biological properties of chitin/polylactide(PLA)/hydroxyapatite (HAP) composites cast using ionic liquid solutions. International Journal of Biological Macromolecules, 151: 1213-1223.

Coelho, C.C., Grenho, L. Gomes, P.S. Quadros, P.A. and Fernandes, M.H. 2019. Nano-hydroxyapatite in oral care cosmetics: characterization and cytotoxicity assessment. Scientific Reports – Nature, 9(1): 1-10.

Curkovic, L., Zmak, I. Kurajica, S. Tonkovic, M.E. Sokcevic, Z. and Renjo, M.M. 2017. From eggshells biowaste to hydroxyapatite biomaterial. Materials Science & Engineering Technology, 48(8): 797-802.

Dan, P., Sundararajan, V. Ganeshkumar, H. Gnanabarathi, B. Subramanian, A.K. Venkatasubu, D. Ichihara, S. Ichihara, G. Mohideen, S.S. 2019. Evaluation of hydroxyapatite nanoparticles-induced in vivo toxicity in Drosophila melanogaster. Applied Surface Science, 484: 568-577.

Es-saddik, M. Laasri, S. Taha, M. Laghzizil, A. Guidara, A. Chaari, K. Bouaziz, J. Hajjaji, A. and Nunzi, J.M. 2021. Effect of the surface chemistry on the stability and mechanical properties of the zirconia-hydroxyapatite bioceramic. Surfaces and Interfaces, 23: 1-7.

Ficai, A., Andronescu, E. Voicu, G. and Ficai, D. 2011. Advances in Composite Materials for Medicine and Nanotechnology In book: Advances in Composite Materials for Medicine and Nanotechnology, 1-32.

Gomes, D.S., Santos, A.M.C. Neves, G.A. and Menezes, A. 2019. A brief review on hydroxyapatite production and use in biomedicine. Ceramica, 65: 282-302.

Hanora, A. and Mostafa, M.M. 2021. Synthesis of silica/hydroxyapatite nanocomposite by mechanochemical method. Research Square, 1-15.

Hariani, P.L. Muryati, and Said, M. 2019. Kinetic and thermodynamic adsorption of nickel (II) onto hydroxyapatite prepared from snakehead (*Channa striata*) fish bone. Mediterranian Journal of Chemistry, 9(2): 85-94.

Hariani, P.L., Riyanti, F. Fatma, Rachmat, A. and Herbanu, A. 2020. Removal of Pb(II) using hydroxyapatite from Golden Snail shell (*Pomacea canaliculata* L) modified with silica. Molekul, 15(2): 130-139.

Hubadillah, S.K., Othman, M.H.D. Tai, Z.S. Jamalludin, M.R. Yusuf, N.K. Ah, mad, A. Rahman, M.A. Jaafar, J., Kadir, S.H.S.A. and Harun, Z. 2020. Novel hydroxyapatite-based bioceramic hollow fiber membrane derived from waste cow bone for textile wastewater treatment. Chemical Engineering Journal, 379: 1-12.

Hsu, C.S., Haag, S.L. Bernards, M.T. and Li, Q. 2021. Effect of chloride substitution on physical, mechanical, and biological properties of hydroxyapatite. Ceramic Internasional, 47: 13207-13215.

Ibrahim, M., Labaki, M. Giraudon, J.M. and Lamonier, J.F. 2020. Hydroxyapatite a multifunctional material for air, water and soil pollution control: a review. Journal of Hazardous Materials, 383: 1-18.

Jouda, N.S. and Essa, A.F. 2021. Preparation and study of the structural, physical and mechanical properties of hydroxyapatite nanocomposite. Materials Today: Proceedings, 1-7

Kailasanathan, C. and Gangadharan, T. 2016. Influence of Bio Inert Silica on Mechanical Properties and their dependence on Porosity of Nanocrystalline based Hydroxyapatite/Gelatin Composites Synthesized by coprecipitation Method. Journal of the Australian Ceramic Society. 52(2): 52 – 61.

Latifi, S.M. 2012. Preparation and characterization of hydroxyapatite-silica composite nanopowder. International Journal of Modern Physics: Conference Series, 5: 630-637.

Noviyanti, A.R., Rahayu, I. Fauzia, R.P. and Risdiana. 2021. The effect of Mg concentration to mechanical strength of hydroxyapatite derived from eggshell. Arabian Journal of Chemistry, 14: 1-7.

Obada, D.O., Dauda, E.T. Abifarin, J.K. Arhin, D.D. and Bansod, N.D. 2020. Mechanical properties of natural hydroxyapatite using low cold compaction pressure: effect of sintering temperature. Materials Chemistry and Physics, 239: 1-9.

Pal, A., Hadagalli, K. Bhat, P. Goel, V. and Mandal, S. 2019. Hydroxyapatite-a promising sunscreen filter. Journal of the Australian Ceramic Society, 56: 345-351.

Pamungkas, A., Dhelika, R. and Saragih, A.S. 2019. Synthesis of hydroxyapatite from tenggiri (Scomberomorus commersonii) fish bone: finding on experiment and processes. AIP Conference Proceedings, 2092: 2-10.

Pighinelli, L. and Kucharska, M. 2013. Chitosan-hydroxyapatite composites. Carbohydrate Polymers, 93: 256-262.

Pu'ad, N.M., Koshy, P. Abdullah, H. and Idris, M. 2019. Syntheses of hydroxyapatite from natural source. Heliyon, 5(5): 1-14.

Ramesh, S., Aw, K.I. Tolouei, Amiriyan, M. Tan, C.Y. Hamdi, M. Purbolaksono, J. hassan, M.A. and Teng, W.D. 2013. Sintering properties of hydroxyapatite powder prepared using different methods. Ceramic Internasional, 39: 111-119.

Rho, J.Y., Tsui, T.Y. and Pharr, G.M. 1997. Elastic properties of humancortical and trabecular lamellar bone measured by nanoindentation. Biomaterials, 18: 1325-1330.

Sadeghazade, S., Emadi, R. and Ghomi. 2015. Mechanical alloying synthesis of forsterite-diopside nanocomposites powder for using in tissue engineering. Ceramic Silikaty, 59(1): 1-5.

Saha, B., Yadav, S.K. and Sengupta, S. 2018. Synthesis of nano-Hap prepared through green route and its application in oxidation in oxidative desulfurization. Fuel, 222: 743-752;

Shakir, M., Jolly, R. Khan, A.A. Ahmed, S.S. Alam, S. Rauf, M.A. Owais, M. and Farooqi, M.A. 2018. Resol based chitosan/nano-hydroxyapatite nanoensemble for effective bone tissue engineering. Carbohydrate Polymers, 179: 317-327.

Szczes,A., Holysz, L. Chibowski, E. 2017. Synthesis of hydroxyapatite for biomedical applications. Advances in Colloid and Interface Science, 249: 321-330.

Taha, M.A., Youness, R.A. and Ibrahim, M. 2020. Biocompatibility, Physico-chemical and mechanical properties of hydroxyapatite-based silicon dioxide nanocomposite for biomedical applications. Ceramics Internasional, 46: 23599-23610.

Thian, E.S., Huang, J. and Best, S.M. 2006. The response of osteoblasts to nanocrystalline silicon-substituted hydroxyapatite thin film. Biomaterials, 27: 2692-2698

Xiao, H., Huang, W. Xiong, K. Ruan, S. Yuan, C. Mau, G. Tian, R. Zhou, S. She, R. and Ya, P. 2019. Osteodral repair using scaffolds with gradient pore size constructed with silk fibroin, chitosan, and nano-hydroxyapatite. International Journal of Nanomedicine,14: 2011-2027.

Xu, H.K.K., Smith, D.T. and Simon, C.G. 2004. Strong and bioactive composites containing nano-silica-fused whiskers for bone repair. Biomaterials, 25: 4615-4626.

Wang, K., Wang, M. Wang, Q. Lu, X. and Zhang, X. 2017. Computer simulation of proteins adsorption on hydroxyapatite surfaces with calcium phosphate ions. Journal of the European Ceramic Society, 37(6): 2509-2520.

Witoon, T. 2011. Characterization of Calcium Oxide Derived from Waste Eggshell and Its Application as CO_2 Sorbent. Ceramics International, 37: 3291-3298.